https://ntrs.nasa.gov/search.jsp?R=20080031613 2019-08-30T04:55:32+00:00Z

Stereoscopic Imaging in Hypersonics Boundary Layers using Planar Laser-Induced Fluorescence

Paul M. Danehy*, Brett Bathel†, Jennifer A. Inman‡, David W. Alderfer§, Stephen B. Jones**

NASA Langley Research Center, Hampton VA, 23681-2199

Stereoscopic time-resolved visualization of three-dimensional structures in a hypersonic flow has been performed for the first time. Nitric Oxide (NO) was seeded into hypersonic boundary layer flows that were designed to transition from laminar to turbulent. A thick laser sheet illuminated and excited the NO, causing spatially-varying fluorescence. Two cameras in a stereoscopic configuration were used to image the fluorescence. The images were processed in a computer visualization environment to provide stereoscopic image pairs. Two methods were used to display these image pairs: a cross-eyed viewing method which can be viewed by naked eyes, and red/blue anaglyphs, which require viewing through red/blue glasses. The images visualized three-dimensional information that would be lost if conventional planar laser-induced fluorescence imaging had been used. Two model configurations were studied in NASA Langley Research Center's 31-Inch Mach 10 Air Wind tunnel. One model was a 10 degree half-angle wedge containing a small protuberance to force the flow to transition. The other model was a 1/3-scale, truncated Hyper-X forebody model with blowing through a series of holes to force the boundary layer flow to transition to turbulence. In the former case, low flowrates of pure NO seeded and marked the boundary layer fluid. In the latter, a trace concentration of NO was seeded into the injected N_2 gas. The three-dimensional visualizations have an effective time resolution of about 500 ns, which is fast enough to freeze this hypersonic flow. The 512x512 resolution of the resulting images is much higher than high-speed laser-sheet scanning systems with similar time response, which typically measure 10-20 planes.

I. Introduction

Understanding the transition from laminar to turbulent flow is critical in designing and operating hypersonic vehicles. In air-breathing vehicles, turbulent boundary layer flow is desired to improve fuel-air mixing, increase mass capture, and reduce the susceptibility to flow separations within the engine.[1] For entry vehicles, transitional and turbulent flow can cause many times higher heat transfer to the vehicle than laminar flow. Concerns over such increased heating led to an unplanned spacewalk to remove *gap fillers* (material inserted between high-temperature reusable surface insulation—HRSI—tiles) protruding from the orbiter's windward surface on STS-114.[2] Thus, having accurate theoretical models and engineering tools to predict transition onset are critically important for hypersonic vehicle design and operation.

The development of new fluid mechanical predictive tools is currently inhibited by a lack of detailed experimental visualization and quantitative data characterizing the flow structures in a transitional flow. Transitional and turbulent flowfields are highly three dimensional. Measurement techniques to visualize and quantify these three-dimensional flow structures are highly sought after. Planar imaging techniques such as Raman, Rayleigh, and Mie scattering, particle image velocimetry (PIV), laser induced incandescence (LII) and planar laser-induced fluorescence (PLIF) typically only measure a slice through these structures. These planar measurements provide an incomplete understanding of the size and shape of structures in transitional and turbulent flows. In

* Research Scientist, Advanced Sensing and Optical Measurement Branch, MS 493, AIAA Associate Fellow.
† PhD Student, University of Virginia, Charlottesville VA and Graduate Student at the National Institute of Aerospace, Hampton VA, AIAA Student Member.
‡ Research Scientist, Advanced Sensing and Optical Measurement Branch, MS 493, AIAA Member.
§ Research Scientist, Advanced Sensing and Optical Measurement Branch, MS 493.
** Technician, Advanced Sensing and Optical Measurement Branch, MS 493.

various gas-flow applications, these same techniques have been implemented with a laser sheet that sweeps across the flowfield while multiple images are acquired during a time period in which the flow is effectively frozen.[3-10] These images can be reconstructed in post processing to resolve the three-dimensional flow structures. However, to obtain fast time response in high-speed flows, researchers have demonstrated or proposed laser-scanning systems that would measure ~50 slices of the flow in tens of microseconds,[10] 10 to 20 slices in ~1 microsecond,[4,5,8] and 6 slices in tens of nanoseconds.[6] Generally speaking, faster time resolution results in lower image resolution in the third dimension of the volume being studied. In hypersonic flows, typically travelling faster than 1 km/s and occasionally up to 5 km/s or higher, the flow structures convect and evolve appreciably in time scales of 1 microsecond or shorter. Thus, sub-microsecond imaging capabilities are required. In addition, the spatial scales in hypersonic transitional and turbulent boundary layers are small and the structures can be complicated and numerous, so a high-resolution and high-magnification imaging system is required. Current laser-sheet scanning technologies cannot provide both high spatial resolution in all three dimensions and fast time response required to resolve these flows. Furthermore, laser-sheet scanning systems often use custom laser systems and expensive multiple-image camera technology. These experiments are complex, requiring sophisticated scanning mechanisms and accurate synchronization of laser and camera technologies.

Tomography[11,12] and tomographic reconstruction from multiple-view holographic interferometry[13] are additional candidate methods for visualizing flow structures with sub-microsecond time resolution. However, tomographic systems require many projections of the flowfield in order to produce high-resolution flow images. This makes such systems complex and expensive to set up and operate. Also, they require optical access from many different directions – ideally a 360 degree view around the flow. Another approach is stereoscopic photography.[14-16] Such an approach has been used successfully to visualize turbulent flow structures in combustion environments by seeding fine titanium dioxide particles into the combustion gases. When the particles heat up, they radiate and the radiation is captured by a pair of cameras or a camera equipped with a stereoscopic viewing adaptor. Computer reconstructions of these flows allow the flame shape and surface area to be determined. This approach is limited to high temperature environments and relatively long time resolutions of 1 millisecond. At shorter exposure times the intensity of the captured emission becomes too low.

Previously, we have used nitric oxide (NO) PLIF to obtain planar slices through transitional flowfields in a hypersonic blowdown wind tunnel using a thin (< 1mm) laser sheet.[17] In this paper we use a thick (~10 mm) laser sheet to excite a volume of gas seeded with NO. Fluorescence from the NO is collected by a pair of identical intensified CCD cameras, mounted side-by-side and viewing the same region. Subsequent image processing allows the viewer to see the three-dimensional flow structures. There are several advantages of the new method. Most importantly, the time response is short enough to freeze the rapidly-changing hypersonic flow structures. Second, the resolution of the final stereoscopic images is determined by the resolution of the cameras being used; in this case 512x512. Third, custom-built lasers or camera components are not required, nor is a scanning mechanism, thereby decreasing the cost and complexity of the experimental setup. Fourth, the setup is very easy to implement if already performing conventional PLIF imaging: it requires a slight modification to the sheet-forming optics and a second imaging camera (or a stereoscopic viewing adaptor mounted on a single camera). The main drawback of the technique is that extracting three-dimensional spatial information from the obtained images is difficult, though possible.[14-16] Also, the flow must be seeded with a fluorescing gas, or the fluorescent gas must be naturally present. In addition to the stereoscopic imaging capability, the thick-laser-sheet imaging method is shown to be a useful tool in its own right, allowing improved views of transitional and turbulent structures compared to thin planar slices of the flow.

II. Experiment and Analysis Description

The experiments were performed in the 31-Inch Mach 10 Air Tunnel at NASA Langley Research Center. The test apparatus consisted of three main components: the test articles, the wind tunnel facility and the PLIF system. The analysis includes image processing and subsequent rendering in a three-dimensional software environment. These procedures are summarized briefly in this section with references describing where more details can be found. Methods used to post-process the PLIF images are also described in this section.

A. Test Articles

Two different test articles were investigated to demonstrate the new stereoscopic imaging approach. Computer renderings of these models are shown in Fig. 3. One test article was a 20-degree full angle, wedge-shaped model. One of the flat surfaces of this model was oriented at a 20° angle with respect to the oncoming flow. On this surface, we attached different shaped protrusions to trip the flow from laminar to turbulent. The results shown in

this paper were obtained with a triangular trip, swept at a 45° angle to the upcoming flow, further described in Reference 17. The boundary layer trip was attached 75.4 mm (2.97 in) downstream of the sharp leading edge of the model. NO was seeded into the flow through a 11 mm (0.43 in) long by 0.81 mm (0.032 in) wide slot. The upstream edge of the slot was located 29.4 mm (1.16 in) downstream of the leading edge. Pure NO was supplied through a mass flow controller to a plenum below this slot and the NO then passed through the slot into the flow. Flow rates between 0.3 and 1.0 standard liters per minute (slpm) were used, corresponding to flow velocities issuing from the slot of about 10 to 60 m/s, depending on the flowrate, model angle of attack, and tunnel operating conditions. These flow velocities are much lower than the 1,250 m/s flow velocity calculated at the edge of the boundary layer for these conditions. PLIF images obtained for 0.3 and 1.0 slpm while holding everything else constant were very similar, except that the signal-to-noise ratio of the images was lower in the lower flowrate case. Since the size and shape of the flow structures didn't change when the flowrate changed by over a factor of 3, this implies that the seeding method is non-perturbative. In fact, these low flow rates were used to minimize perturbations to the flow, unlike testing with the Hyper-X model (described in the next paragraph) where the much larger NO-seeded N_2 injection rates were intended to perturb the flow. The injected NO diffused into the boundary layer, thereby marking the boundary layer fluid. This fluid then passed downstream over the trips and became transitional or turbulent. Three quarters of the way through each run, an additional 5 slpm of pure N_2 was supplied to the flow through the slot. This increased flowrate purposely perturbed the flow, altering the flow structures downstream, thereby producing additional flow structures to demonstrate the stereoscopic imaging technique. Further details of this model can be found in Reference 17.

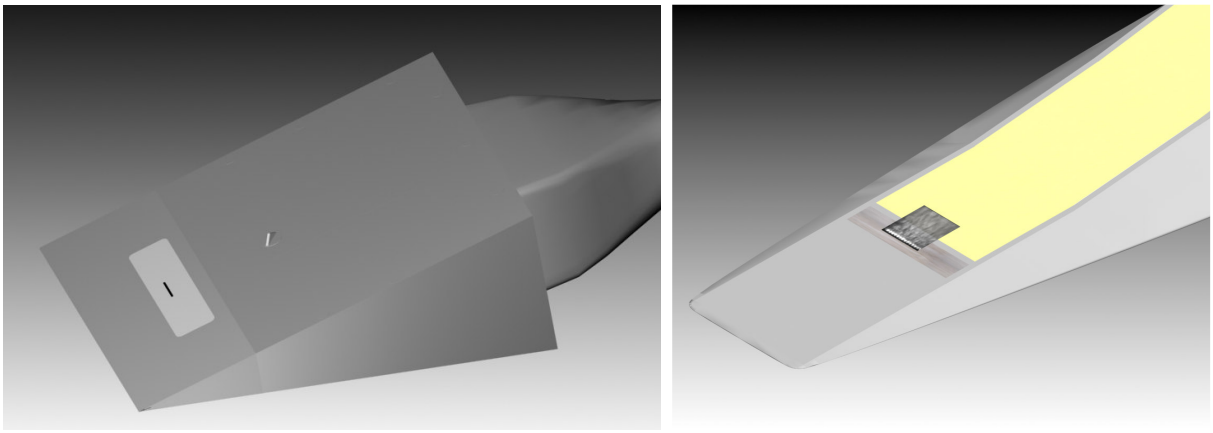

Figure 1 Test articles used in the experiment, showing the wedge model (left) and Hyper-X forebody model (right). The Hyper-X model shows a PLIF image superimposed on the region imaged by the cameras in this experiment.

The other test article investigated in this study was a 1/3-scale, truncated Hyper-X vehicle forebody, which has a square leading edge with a 0.010 in. radius, followed by a series of flat plates (ramps) arranged to compress the flow upstream of a scramjet engine inlet. The first plate is oriented at a 4.5° degree angle with respect to the oncoming flow. Midway down this plate is a cavity for installing different inserts containing either protrusions or holes for blowing gas. An insert containing 17 spanwise blowing orifices was used in this experiment to actively force the flow to become turbulent while also seeding the flow with NO for the visualization system. A plenum underneath the insert was connected to external supplies of N_2 and NO. Mass flow controllers allowed various flow rates and relative NO to N_2 concentrations to be supplied to these orifices, ranging from 0.7 to 49.7 slpm, with typical NO concentrations of a few percent at the higher flow rates. For further details of this model, see References 1 and 18.

B. Wind Tunnel, Tunnel Operating Conditions and Data Acquisition

The 31-Inch Mach 10 Air Tunnel is an electrically-heated blowdown facility located at NASA Langley Research Center in Hampton, Virginia, USA. Reference 19 details this facility, a brief summary of which is provided here. The facility has a nominal Mach number of 10 and a 31-inch square test section and operates on electrically heated, compressed air. Large windows, transparent in the ultraviolet down to approximately 190 nm, form three walls (including top and bottom) of the test section with the fourth wall formed by the model injection system. In both experiments, the model was side-mounted to this fourth wall. Run durations for the current tests were about one minute. The nominal stagnation temperature was 1,005 K (1,350° F) for all tests described herein. Two different facility stagnation pressures, P_0, were used: 4.96 MPa (720 psia) and 9.31 MPa (1350 psia). The two operating pressures simulate freestream unit Reynolds numbers of 1 million per foot and 1.9 million per foot, respectively.

Further details of the flow properties at these conditions can be found in Hollis et al.[20] or can be requested from the authors.

The normal sequence of operation was to begin NO flow prior to beginning a wind tunnel run so the flow rates could establish. Data acquisition was started upon injection of the model into the wind tunnel and image acquisition was then initiated. An output signal from the intensified CCD indicated to the data acquisition system that the PLIF image acquisition had begun. For thin-laser-sheet PLIF imaging, a remote manual translation stage trigger could be used to start a sweep of the laser sheet across the model for three-dimensional flow visualizations. For thick-laser-sheet imaging, the position of the sheet was held fixed.

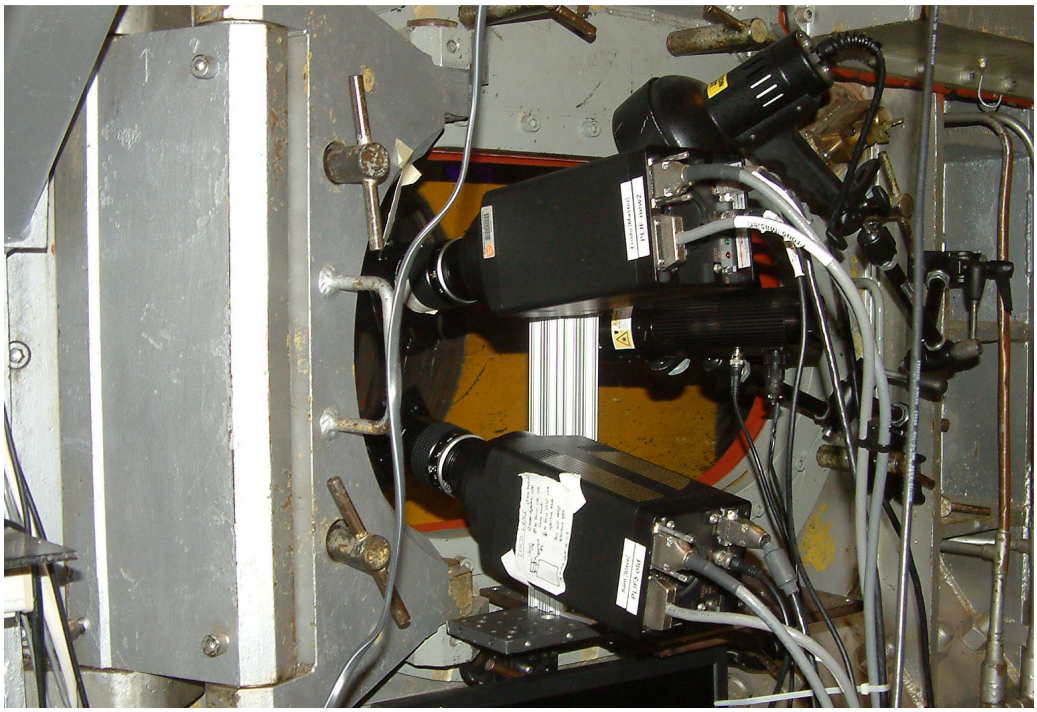

Figure 2 Photograph of camera setup during the wedge model investigation, showing the cameras oriented in the vertical plane. Flow is from left to right in the wind tunnel. For the Hyper-X test, the cameras were in the horizontal plane.

C. Planar Laser-Induced Fluorescence (PLIF) Imaging System

The PLIF system consisted primarily of the laser system, beam-forming optics and the dual-camera detection system. The laser system had a Spectra Physics Pro-230 Nd:YAG pump laser, a Quanta Ray PDL-2 tunable pulsed dye laser, and a Quanta Ray WEX wavelength extender, all operating at 10 Hz and with ~10 ns pulse duration. The laser output was tuned to a wavelength of 226.256 nm, chosen to excite the strongly fluorescing spectral lines of NO near the Q_1 branch head. Lenses formed the laser beam into a sheet. A pair of Princeton Instruments PIMAX-2 intensified CCD cameras acquired images. Both cameras used Nikon 105 mm focal length, F/4.5 UV Nikkor lenses. Flow visualization images were acquired at 10 Hz with a 1 μs camera gate and a spatial resolution of up to 11 pixels/mm. So-called *dotcards* (a flat card marked with evenly spaced dots) were used to determine image magnification in post-processing and for correcting perspective and lens distortion as in previous work.[21]

Typically, when performing NO PLIF flow visualization, the 10 mm diameter UV laser beam was formed into a thin sheet of light using first a cylindrical lens and then a long-focal-length spherical lens. The resulting sheet was collimated and had a cross section of 0.5 mm x 70 mm. This light sheet excited NO molecules, causing fluorescence, and a single camera oriented normal to the sheet captured the fluorescence, allowing for visualization of a slice of the flowfield. By translating the laser sheet, visualization was possible at different locations in the flow, thereby visualizing flow structures that developed and evolved both along and away from a surface. This approach was used in previous work to study three-dimensional structures.[23] In the present experiment, a +72 mm focal length cylindrical lens was placed in the collimated UV beam about 0.6 m from the imaging region to expand the beam in one direction. This resulted in a slightly diverging laser sheet with a width of about 70 mm and a thickness of about 10 mm. Since the laminar boundary layer thickness, as computed using the LAURA (Langley Aerothermodynamic Upwind Relaxation Algorithm) CFD code,[17] is 1-2 mm for the conditions studied here, the 10

mm thick sheet illuminated the entire NO-seeded region. Figure 2 shows a photograph of the cameras mounted to the side of the wind tunnel, viewing the wedge model through the window. In the wedge model test, the two cameras had an angular separation of 12±2 degrees. They were oriented in the vertical plane about 27 inches from the model surface, and approximately normal to the streamwise direction of the wind tunnel flow. In the Hyper-X forebody test, the two cameras had a similar angular separation of about 12±2 degrees and were placed about 22 inches from the model. However, their orientation was different, as the cameras were both in the horizontal plane, with one camera pointed slightly upstream and the other slightly downstream, while imaging the same region on the model. Further details of the mobile NO PLIF system and its use in NASA Langley Research Center's 31-Inch Mach 10 Air Tunnel can be found in Refs. 21, 22 and 23.

D. PLIF Flow Visualization Image Processing

For the wedge-model test, the raw, grayscale images were used without smoothing, background subtraction, or laser sheet normalization. For the Hyper-X data, a background image was subtracted from single-shot PLIF images. They were corrected for spatial variations in laser sheet intensity using the method described in Reference 18. A false color table was not applied in either case to avoid possible interference with the red/blue anaglyph visualizations. As in previous work, the Hyper-X PLIF images were corrected to remove lens and perspective distortion (see Ref. 21). This step was not taken with the wedge model images.

E. Virtual Diagnostics Interface (ViDI)

The Virtual Diagnostics Interface (ViDI)[24] is a software tool, developed at NASA Langley Research Center that provides unified data handling and interactive three-dimensional display of experimental data and computational predictions. It is a combination of custom-developed software applications and Autodesk® 3ds Max®, a commercially available, CAD-like software package for three-dimensional rendering and animation.[25] ViDI technology can be applied to three main areas: 1) pre-test planning and optimization; 2) visualization and analysis of experimental data and/or computational predictions; and 3) establishment of a central hub to visualize, store and retrieve experimental results. For this experiment, ViDI was used for post-test visualization of the PLIF images obtained with the Hyper-X forebody model only. To allow the stereoscopic images to be visualized in the CAD environment, images from both cameras were imported and overlaid on the model. These PLIF images had been processed as described in the previous section. Many images were scaled and overlaid on the model using dotcard images. Two virtual cameras were created in the CAD environment, closely replicating the positions of the two cameras in the experiment. Renderings of the model and the image plane were generated from the perspective of each of these virtual cameras. When these renderings were made, the experimental image data from the left (actual) camera was used for the left virtual camera rendering and vice versa.

F. Stereoscopic Image Processing

The raw images (in the case of the wedge model) and the CAD renderings (in the case of the Hyper-X model) were then imported into the MATLAB®-based subroutine *anaglyph()* version 2.0,[26] which displayed image pairs for stereoscopic viewing. This subroutine could be run in a loop to process multiple images to create movies or montages, as shown below. Montages were generated using the *Image:Stacks:Make Montage…* menu option in the ImageJ program, available from the National Institute of Health. Two different types of image pairs were generated: so-called *cross-eyed viewing* pairs and red/blue anaglyphs. Cross-eyed viewing image pairs are displayed with the image obtained by the left camera shown on the right side, and the image obtained by the right camera shown on the left side. When the viewer's eyes are crossed, the right sees the left image and the left eye sees the right image. If the eyes are over-crossed, four unfocused images are seen. When crossed the appropriate amount, the two central images will appear to overlap. As this central image is brought into focus (with the images to either side remaining unfocused), a three-dimensional effect is observed without the need for specialized eyewear. Red/blue anaglyphs were also produced at the same time. These images must be viewed through glasses having a red filter on the left eye and a blue filter on the right eye to produce the stereoscopic effect. In both cases, the three-dimensional reconstructions occur in the viewer's brain.

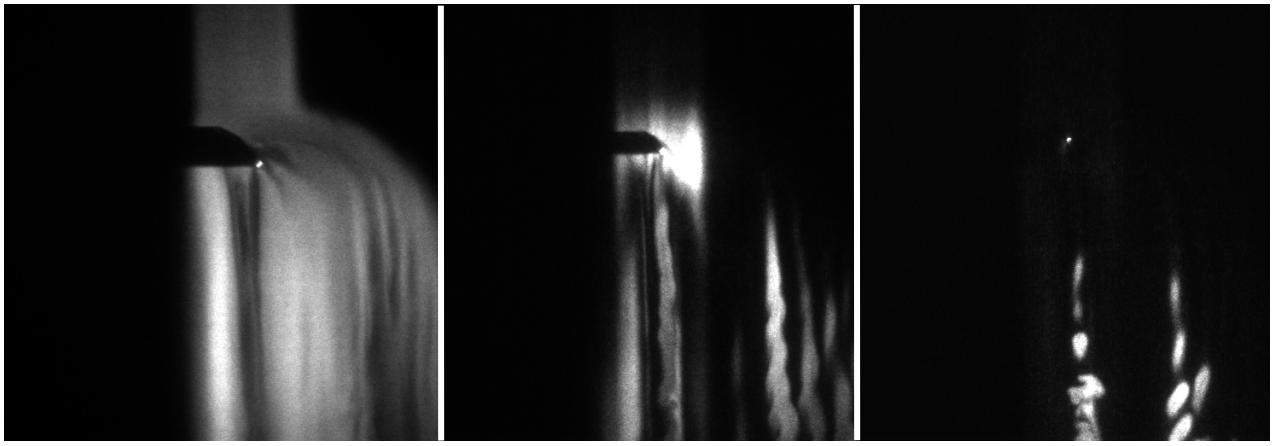

Figure 3 Thin-laser-sheet NO PLIF images of flow over a single triangular roughness element swept at a 45° angle. Flow is from top to bottom. The left image was obtained 0.008 in., the middle 0.04 in., and the right 0.08 in. above the plate. The field of view of each image is approximately 2.4 inches square.

III. Results

A. Thin vs. Thick Laser Sheet, Cross-Eyed and Red/blue Anaglyph Viewing

Figure 3 shows NO PLIF images obtained using the conventional thin-laser-sheet approach. The NO-seeded gas flows from top to bottom in the image over a 2-mm high triangular trip. The thin laser sheet (thickness of 0.012 in, or 0.3 mm) was scanned from the surface of the model through and then out of the boundary layer. The top of the trip is just visible in the right image. As Fig. 3 shows, the flow varies significantly depending on height above the plate. The flow is more laminar neat the plate and more unsteady further from the plate. Planar slices of flow structures are obtained with this method, such as the tops of a corkscrew shaped vortex in the right image in Fig. 3.

Figure 4 compares two different methods used to view stereo images obtained using the wedge model. The top row shows the raw images obtained from the two cameras. The image on the left was obtained from the right camera and vice versa. Before discussing stereoscopic imaging in detail, it is worth noting that individually, these thick laser sheet images themselves provide valuable information about the flow. In Fig. 4, the individual images reveal that the flow coming towards the trip is laminar and that the flow just downstream of the trip is also laminar. Since the trip is oriented at a 45° angle with respect to the oncoming flow, some of the seeded gas deflects to the right side of the images. This trip also introduces streaks into the downstream flow, both directly in the wake of the trip and also in the deflected gas. The streaks begin to oscillate and appear to rotate further downtream, taking on a rope-like or corkscrew-shaped structure, possibly indicating vortices. Measurements obtained using a thin laser sheet (Fig. 3) did not show all of these features simultaneously. Instead, the thin laser sheet images showed slices through these flow structures while probing different heights within the boundary layer more precisely. The thin- and thick-laser-sheet approaches are thus complementary.

Several methods exist to visualize stereoscopic images. For example, polarization-sensitive glasses can be worn to view a computer monitor or projection screen in which pairs of stereoscopic images are displayed with crossed polarizations. Another scheme uses specialized eyewear that rapidly switches between transparency and opacity for each eye, alternately. The two stereoscopic images are then displayed in sequence, synchronized with the glasses. Neither of these approaches are appropriate for publication, nor for presentation to large groups because specialized eyewear is expensive and cumbersome to set up. The first method used in this paper is *cross-eyed viewing*. If the viewers eyes are crossed slightly, the two top images in Fig. 4 will appear to merge, and can be interpreted by the brain as two different views of the same object, resulting in a perceived three-dimensional effect. There are advantages to visualizing stereoscopic images using this cross-eyed viewing method. First, no additional or specialized eyewear is required. Second, since the red and blue colors are not being used to transmit three-dimensional information, a false color scale could be applied to these images to enhance certain flow details if desired. Unfortunately, many people cannot observe the three-dimensional effect from cross-eyed viewing easily.

Red/blue anaglyphs are the second method used to display stereoscopic images in this paper. The bottom left image in Fig. 4 shows the same data as in the top row, but in the form of an anaglyph. The anaglyph in the bottom right hand corner of Fig. 4 shows an average of 16 images. Viewing glasses with a red filter over the left eye and a blue filter over the right eye are required to correctly interpret these images.

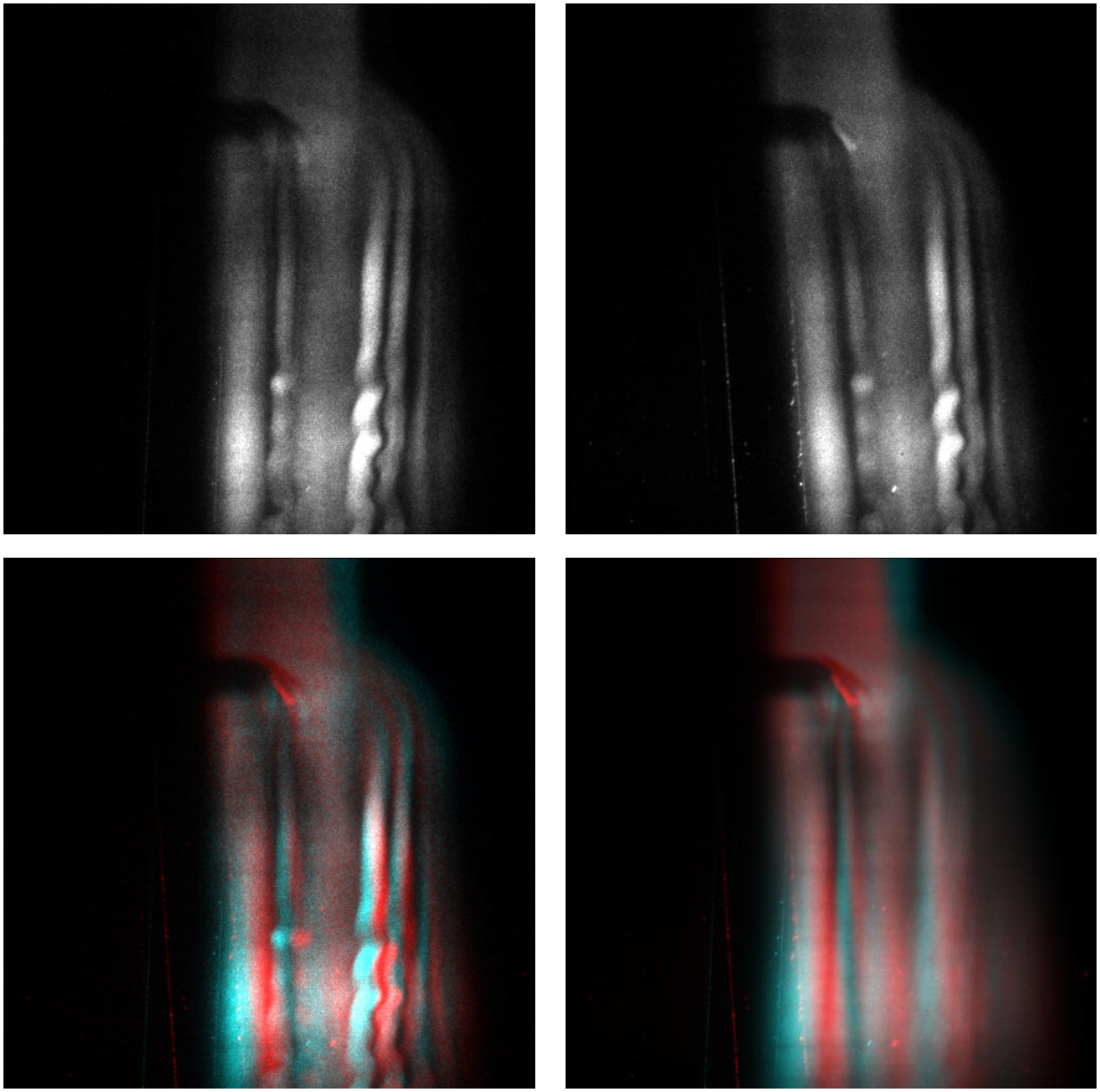

Figure 4 Stereoscopic NO PLIF images of flow over a single triangular roughness element swept at a 45° angle. Flow is from top to bottom. The top row shows images intended to be viewed using the cross eyed viewing method. The bottom-left image shows the same data displayed as a red/blue anaglyph. The bottom-right image shows an average of 16 such red/blue anaglyph images obtained at the same flow conditions, and shown in Fig. 5. The field of view of each image is approximately 2.4 inches square.

When these images are viewed appropriately, the flat plate and the gas flow appear to angle out of the page at the bottom of each image. Upon closer inspection, the three-dimensional shape of the model and flow structures can be observed, such as the triangular trip itself and the corkscrew vortex on the bottom right of the single-shot images. The boundary layer and these downstream vortices are very thin in this experiment, so the angle between the cameras was increased during the setup to exaggerate the three-dimensional effect. This is why the image plane appears so far out of the plane of the paper. The averaged image also shows the three-dimensional effect. Several vertical streaks in the bottom half of the averaged image indicate that the streaks induced by the triangular trip form in approximately the same place, image after image. Since many viewers cannot sense the three-dimensional effect from the cross-eyed images, the rest of the images in this paper use red/blue anaglyphs. Unfortunately, some colorblind viewers will not be able to observe three-dimensional effects in these red/blue anaglyphs.

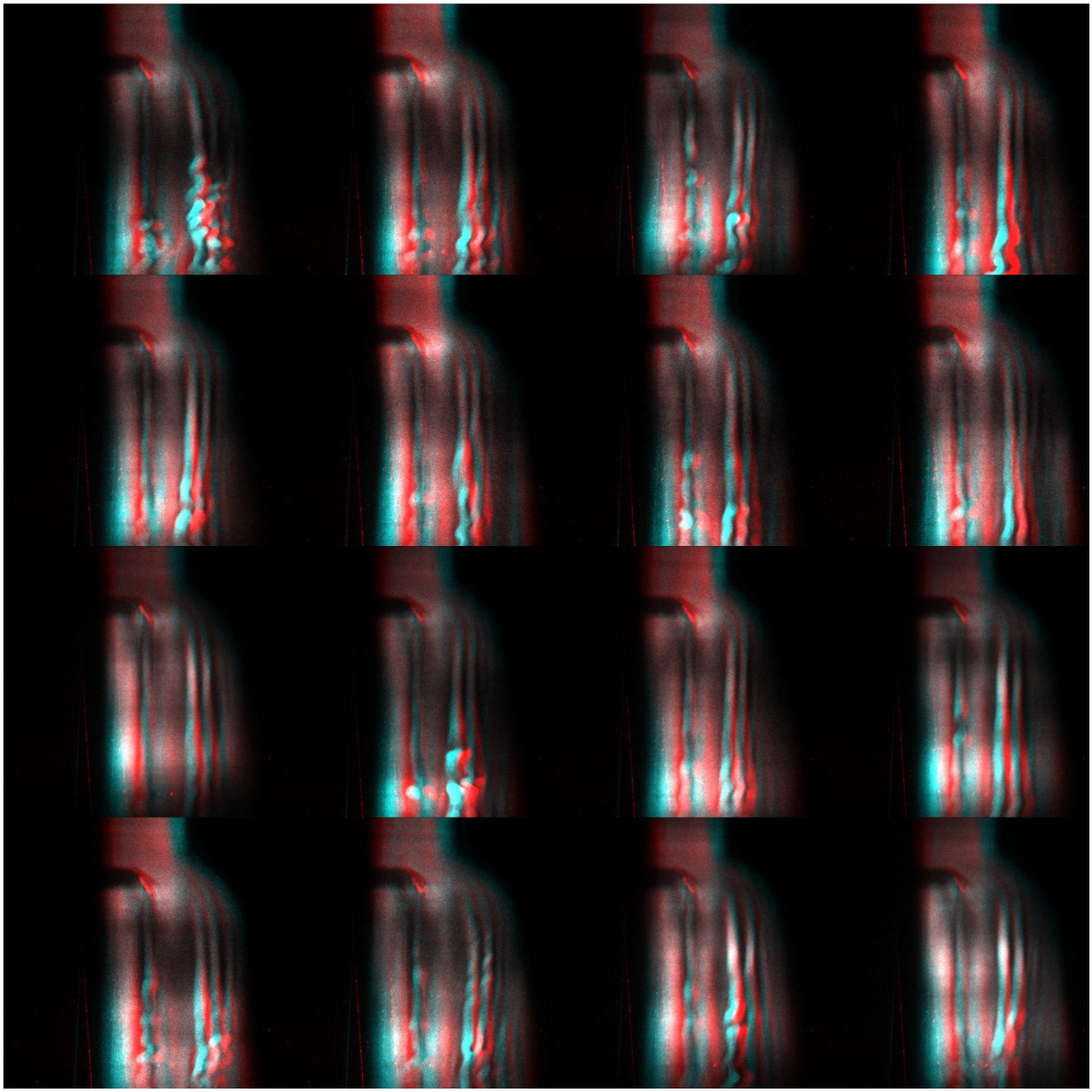

Figure 5. Sixteen single-shot anaglyphs of NO PLIF visualizations for flow over a triangular trip, seeding the flow with 1 slpm of pure NO, P_0 = 4.96 MPa (720 psi). The images were acquired consecutively at a rate of 10 Hz, and so are uncorrelated with each other. Flow is from top to bottom.

B. Wedge-Model Results

Figure 5 shows a series of 16 red/blue anaglyphs for the same operating conditions as Fig. 4. This montage of images indicates a smooth laminar flow upstream of the trip and the intermittent distortions of the streaks (loosely referred to as "transition" hereon) occurring downstream of this trip. Some images show almost no corkscrew-shaped vortices downstream of the trip, while others show corkscrew structures vigorously breaking down into smaller, and seemingly turbulent structures, or merging with adjacent structures. Near the bottom of the top-left image, a tube of seeded gas appears to wrap around another. The two vortices that usually develop on the right side of the images appear to always have the same direction of rotation and they often wobble in sync with each other, indicative of a sinuous mode of streak breakdown. Another observation is that the gas directly downstream of the trip does not develop into as vigorous of corkscrew structures as the gas on the right side of the images that has been

diverted by the trip. The gas directly downstream of the trip appears to breakdown into less organized and smaller scale structures before the gas diverted by the trips to the right side of the images breaks down. Interestingly, some laminar flow persists at the bottom of every image. The influence of streak breakdown is highly localized, at least in this small field of view.

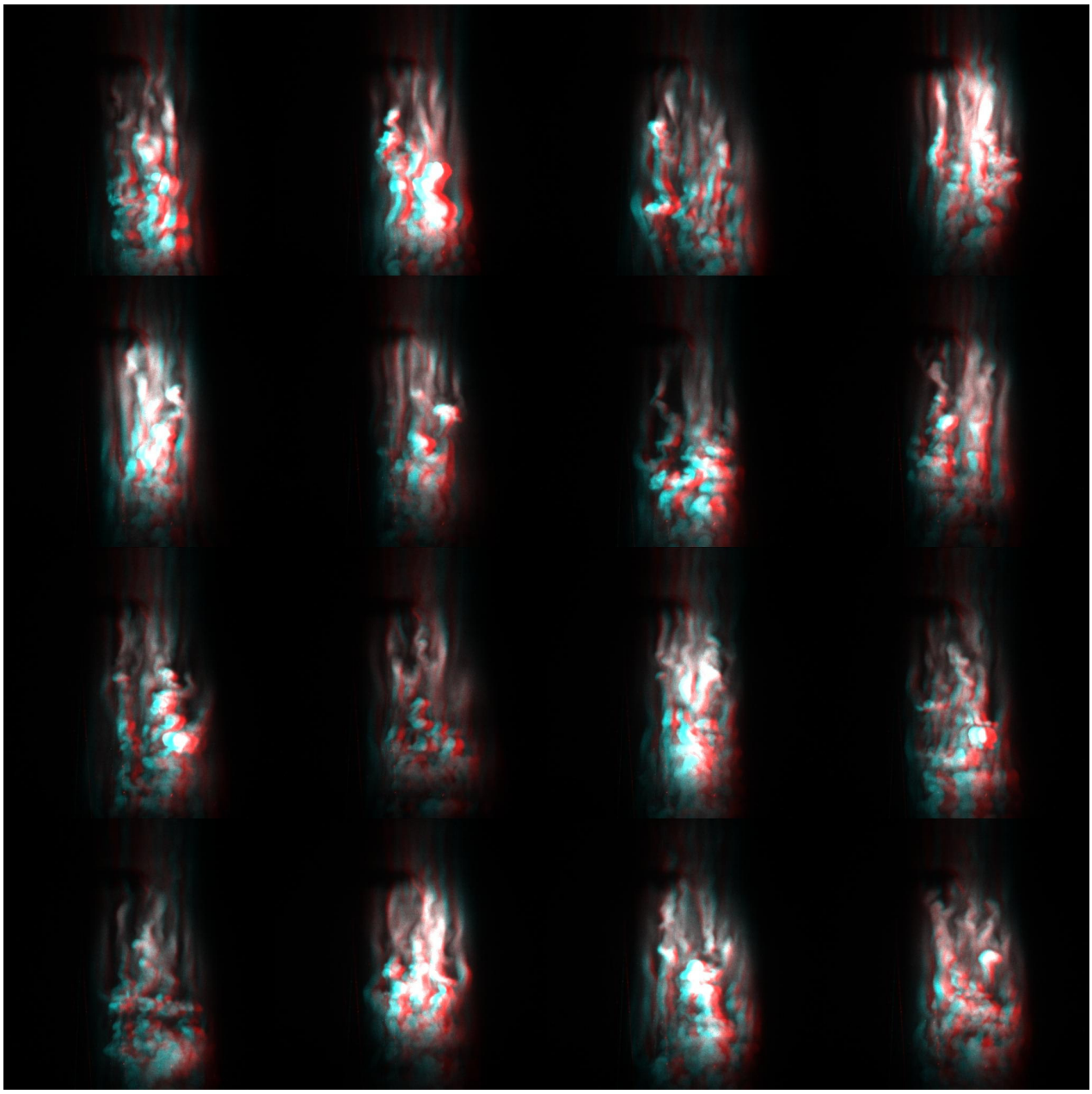

Figure 6: Sixteen single-shot anaglyphs of NO PLIF visualizations for flow over a triangular trip, seeding the flow with 1 slpm of pure NO and 5 slpm of N_2 through the same slot, P_0 = 4.96 MPa (720 psi). Flow is from top to bottom.

In Fig. 5, the 1 slpm flow rate of NO did not cause the boundary layer to transition prior to the trip. In fact, experiments on a smooth flat plate (no trip installed) showed that the 1 slpm rate of injection did not stimulate transition over the full 6-inch length of the flat plate. However, when the total flow rate was increased to 6 slpm by adding 5 slpm of pure N_2 to the injected NO, the flow behavior changed markedly. Figure 6 shows several red/blue anaglyphs for these conditions. Unlike in Fig. 5, streaks are observed in the flow upstream of the trip. Vortices have likely been induced by the injected gas. When these vortices impact the trip, they rapidly begin to break down into much smaller structures. The stereoscopic imagery shows that many of these structures lift off the surface as

they propagate downstream, while others lie closer to the surface. Notably, the trip does not appear to divert as much gas to the right side of each image as compared to Fig. 5.

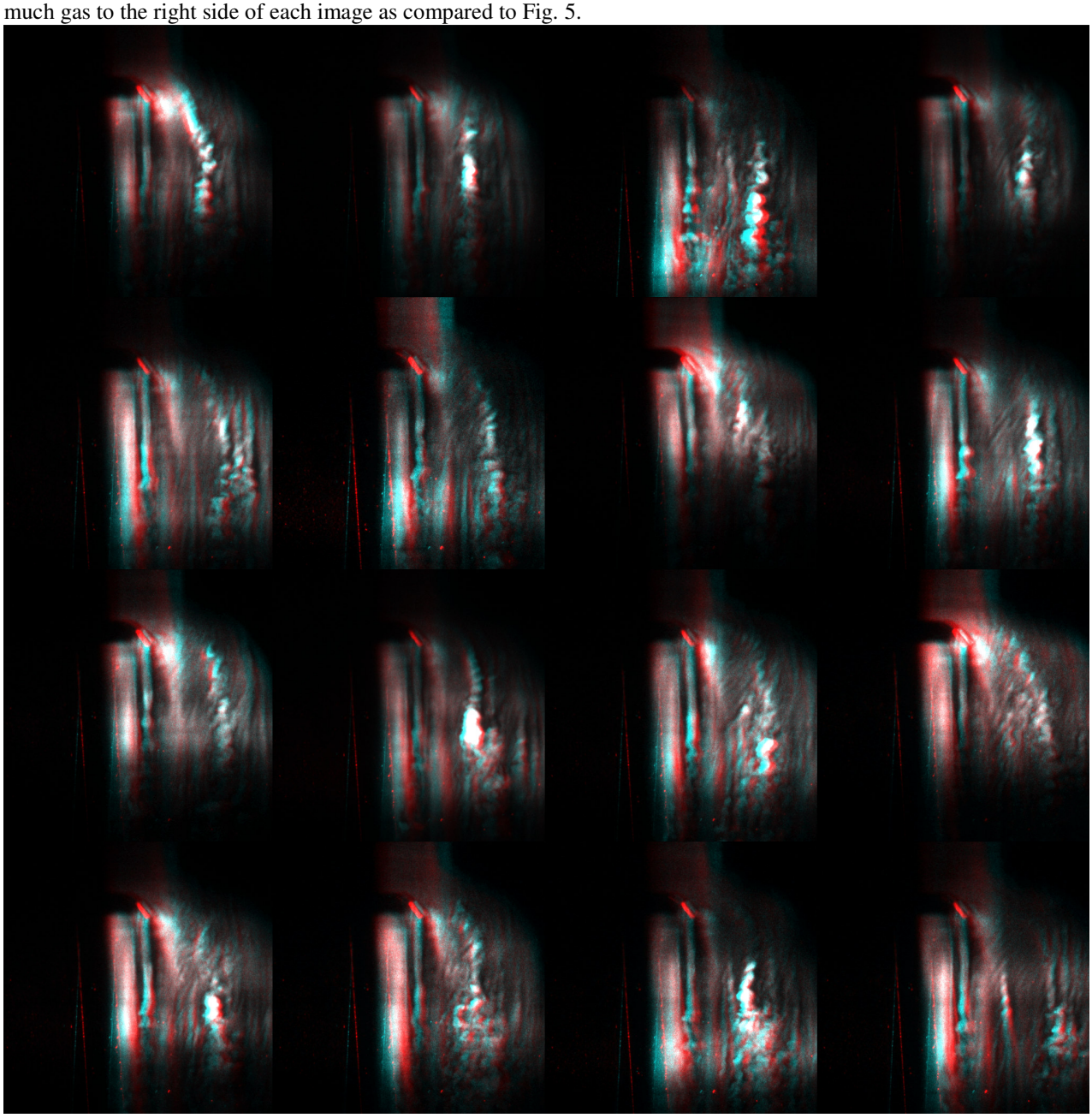

Figure 7: Sixteen single-shot anaglyphs of NO PLIF visualizations for flow over a triangular trip, seeding the flow with 1 slpm of pure NO, for P_0 = 9.31 MPa (1350 psi) causing a Reynolds number about twice as high as in Fig. 5. Flow is from top to bottom.

By varying the tunnel stagnation pressure, P_0, the unit Reynolds number can be changed to study Reynolds number effects. Figure 7 shows the stereoscopic images obtained with the same settings and conditions as presented in Fig. 5 except with roughly twice the Reynolds number. There are numerous similarities between Figs. 5 and 7. The images show laminar flow approaching the swept triangular trip at the top of each image. The flow on the left side of the image stays mostly laminar. The flow directly downstream of the trip shows their transitional behavior, which is qualitatively similar to Fig. 5. However, there are at least three marked differences between Figs. 5 and 7. The first big difference is that the corkscrew-shaped vortices are much more vigorous in Fig. 7. The corkscrew shapes appear to have many more turns - for example six or more compared to two or three typically observed in Fig. 5. Second, diagonal flow structures very close to the surface of the plate appear on the right side of many of the images in Fig. 7. These diagonal features did not appear in the lower Reynolds number case, shown in Fig. 5.

Finally, towards the bottom of the images, the breakdown from unsteady vortices to turbulent flow appears to have progressed further, as evidenced by the smaller scale of the structures compared to Fig. 5.

C. Hyper-X Results

Figure 8 shows stereoscopic PLIF imaging of blowing-induced transition on the Hyper-X forebody model. NO-seeded N_2 was blown through a row of 17 holes oriented in the spanwise direction across the model. This section of the Hyper-X forebody model was effectively a flat plate. The model was oriented at a 2° angle of attack, resulting in a 4.5° plate angle with respect to the oncoming flow. The injection holes are drilled normal to this flat surface and were fed from a plenum inside the model. In this experiment, the two cameras were oriented in the horizontal plane approximately perpendicular to the wind tunnel windows, though at a slight angle to the surface of the model due to the 4.5° angle of inclination. The angular separation between the cameras was also in the horizontal plane. Consequently, flow is from left to right in these images. Unlike the previous data shown in this paper, the ViDI method has been used to superimpose a CAD rendering of the model with the two stereo images. Figure 8 shows the stereoscopic images produced using this method. Three different sections of the model are seen in the cameras' fields of view. To the left is the injection plate, containing the row of holes. To the right is the phosphor-coated plate, which has been colored a dull yellow in these images. Between these is a piece of brushed aluminum which is part of the model body. When viewed with red/blue glasses the model appears to be slightly farther away on the left side of the images and closer to the viewer on the right side of the images, as expected due to the angled surface.

Figure 8(a) shows the resulting images for the lowest flow rate. The gas flow appears to be above the surface of the model. The flow issuing from the orifices appears smooth and round. The static pressure on the surface of the model was measured to be 0.08 psi, ensuring a sufficient pressure ratio to provide choked flow and an underexpanded jet issuing from the holes. The flow downstream of injection is laminar, with the seeded gas diverging and diffusing slightly as it travels downstream. A higher flow rate case in Fig. 8(b) also shows laminar flow downstream. Near the point of injection, the flow has a more complicated structure, showing two lobes typical of a horseshoe vortex. When the flow rate is further increased, as in Fig. 8(c), the injected gas jets increase in diameter due to the increased pressure ratio across the orifice, and transitional structures appear downstream of injection. Corkscrew-shaped vortices appear just downstream of injection. It appears that as these corkscrew-shaped vortices propagate downstream they enlarge and smooth out, possibly dissipating. When the flow rate is increased to the next set point, shown in Fig. 8(d), the gas jets become larger and develop star-shaped patterns. These azimuthal perturbations around the periphery of the jet had been previously identified as sources of instability in transitional, underexpanded jet flows.[27] Indeed, more vigorous transitional structures are observed downstream when compared to the lower-flowrate images. For the highest flowrate tested, shown in Figs. 8(e) and (f), highly underexpanded jets would be expected from the large pressure ratio across the nozzle. Such highly underexpanded jets have low gas density in their cores. Consequently, there is relatively little fluorescence in the jet cores and it is therefore possible to see inside the barrel-shock structure often present in underexpanded jet flows. The azimuthal perturbations around the periphery of the jet make each jet's barrel shock look like a crown.

The stereoscopic effect produced by the combination of two simultaneously acquired images, taken from two slightly different perspectives, enhances the visualization of evolving flow structures. Figure 8(f) shows one of the two images used to create the stereoscopic anaglyph in Fig. 8(e). Comparing these images shows that Fig. 8(f) appears flatter than Fig. 8(e) viewed with the red/blue glasses. In Fig. 8(f) the three dimensional spatial information is collapsed in a single two-dimensional plane. When viewed stereoscopically, the brain re-assembles these collapsed two-dimensional flow structures into a three-dimensional object.

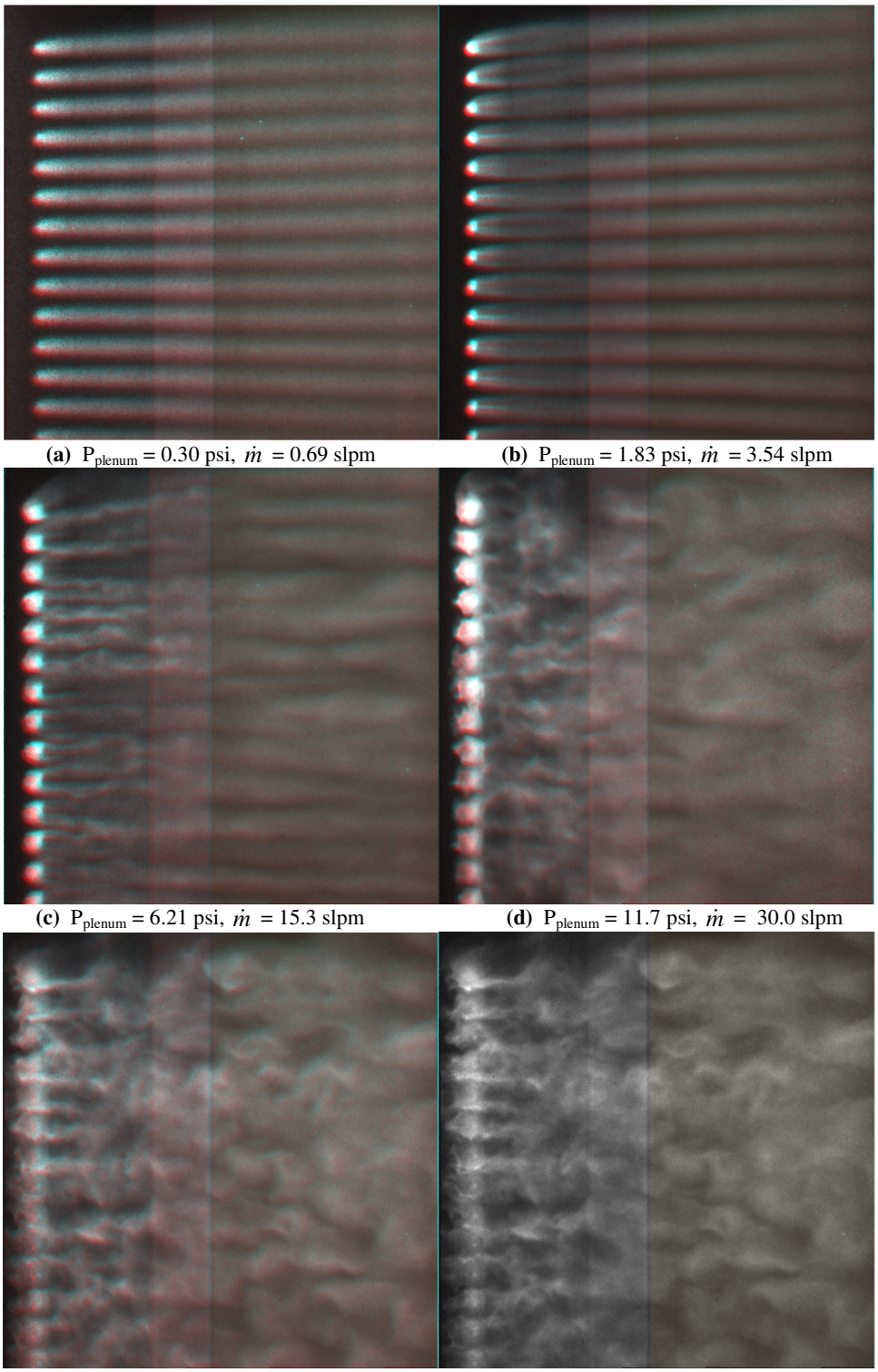

(a) P_{plenum} = 0.30 psi, $\dot{m}$ = 0.69 slpm **(b)** P_{plenum} = 1.83 psi, $\dot{m}$ = 3.54 slpm

(c) P_{plenum} = 6.21 psi, $\dot{m}$ = 15.3 slpm **(d)** P_{plenum} = 11.7 psi, $\dot{m}$ = 30.0 slpm

(e) P_{plenum} = 18.6 psi, $\dot{m}$ = 49.7 slpm (stereo) **(f)** P_{plenum} = 18.6 psi, $\dot{m}$ = 49.7 slpm (right only)

Figure 8: Stereoscopic PLIF visualizations for the Hyper-X model with blowing for four different blowing rates. Flow is from left to right. Image 6(f) is not a stereoscopic anaglyph and shows only the right camera's view.

.

IV. Discussion

When comparing the two data sets, the three-dimensional effect seems much stronger in the wedge model images when compared to the Hyper-X model. The flowfields are relatively similar: both are boundary layer flows on essentially flat plates, both boundary layers are thin, and the angles between the cameras in the distance from the test article were very similar. There were two main differences in the test setups: (1) the cameras were oriented in the vertical plane for the wedge model and were oriented in the horizontal plane for the Hyper-X model and (2) the bisector of the angle between the cameras was nearly perpendicular to the Hyper-X model's surface while the bisector of the angle between the cameras was at a significant angle (perhaps 30°) to the wedge-model's surface.

In the Hyper-X model test, which was performed first, the strongest three-dimensional effect is seen in the highest flowrate image. As the flowrate decreases and the resulting downstream flow becomes more laminar, the resulting images show horizontal tubes of fluorescing gas. The most laminar case produced the weakest three-dimensional effect. These smooth horizontal structures, aligned parallel to a line drawn between the two cameras, does not provide enough structure to allow the brain to reconstruct the image three dimensionally. Stereoscopic viewing is only sensitive to shape or movement in the plane of the viewing cameras. Had the cameras been mounted in a vertical configuration, as shown in Fig. 2, significant curvature would have existed in the plane of the cameras. As a result, the three-dimensional effect would have been much stronger, even for the flow structures presented in Fig. 8(a). When the flow structures become more corrugated at higher flowrates, more curvature exists in the plane of the cameras, and the three-dimensional effect becomes stronger. Since streamline tubular structures were expected in the wedge model test, which was performed after the Hyper-X test, the cameras were mounted in the vertical configuration shown in Fig. 2 to better capture the flow curvature.

The orientation of the bisector of the angle between the cameras, relative to the flat plate, is also an important factor in enhancing the three-dimensional effect. Having additional information and cues in the stereoscopic images helps the brain to create the three-dimensional effect. In the Hyper-X model test, the bisector was nearly normal to the surface of the model. Consequently, the model surface itself only had a slight slope relative to the cameras, and did not provide additional cues to help the brain during reconstruction. We used ViDI in an effort to enhance the three-dimensional effect by adding a slight surface texture to the model so that the views from the two virtual cameras would have more information to aid in the reconstruction process. Despite these efforts, most of the images from the Hyper-X test still look flat in comparison to the wedge model test. In the wedge model test the bisector between the cameras was at a 30° angle with respect to the model surface. Thus, scattered light off the surface of the model allows us to see the steeply angled surface and the brain interprets the images as being highly three-dimensional. Then, once the brain has oriented to this three-dimensional configuration, the fluorescence can more easily be interpreted as being a three-dimensional flow. We believe that the combination of these two camera orientation effects leads to improved stereoscopic viewing for the wedge model.

Regarding the post-test viewing of stereoscopic images, a few observations can be made. The cross-eyed viewing method is less desirable for presenting images in an article. This type of reconstruction cannot be viewed by all and twice as much space is required to display these images compared to read-blue anaglyphs. However, cross-eyed viewing images do not require any specialized eyewear and allow for the application of false color tables to enhance the images.

During the preparation of this paper, it became apparent that the three-dimensional effect was enhanced by placing several stereoscopic images in close proximity to each other, as shown in Fig. 5. This arrangement provides additional clues to the brain to allow it to lock in to the three-dimensional view. Note for example, that the bottom row of images does not exhibit as strong of a three-dimensional effect as those in the middle of Fig. 5. Showing montages of similar stereoscopic images has another advantage: it allows many instantaneous flow visualization images to be presented in a compact form while also enhancing the three-dimensional effect.

The biggest limitation of the method demonstrated in this paper is that the images have not been deconstructed into multiple planar slices by a computer for further analysis. Such deconstructions allow for subsequent reconstruction of the individual planar slices to form a three-dimensional, volume-rendered representation of the flow, viewable from any perspective, and which could be processed to see cross sections of any structures inside the probed volume. This limitation has been somewhat circumvented, using a similar data set obtained from flame luminosity stereoscopic images of turbulent flame structures[14-16] where quantitative reconstruction was performed to determine size, shape, and surface area of the flame. This approach could be used on the current data set. However, if only two views are used, some of the flow structures can be obscured either by the test article or by bright fluorescence nearer to the camera. Lower levels of NO seeding might make the flow features more transparent so that more three-dimensional information can be obtained from two views.[16] Additionally, three or more cameras could be used to visualize obscured regions of the flow.

V. Conclusion

A novel volumetric imaging method has been demonstrated which is less equipment intensive and time consuming to set up than laser-sheet-sweeping 3D imaging systems. This method has sub-microsecond time resolution capable of visualizing hypersonic flows with flow-freezing time response. The three-dimensional information provided by the technique offers much more complete visualization of the flow compared to the thin-laser-sheet method. However, in their current form, the stereoscopic data are less spatially precise than a thin-sheet scanning approach. Compared to conventional thin-laser-sheet imaging methods where all three spatial coordinates are know for each image, the stereoscopic images are somewhat harder to interpret. In the future, it may be possible to recover the spatial information using specialized computational image post-processing. The investigation found that the stereoscopic effect can be enhanced, for these boundary layer flows, by orienting the cameras in the vertical plane and non-orthogonal to the model. Also, when viewing images, the three dimensional effect can be enhanced by displaying several images side-by-side. The new stereoscopic method should be considered as a complementary imaging method to, and not a replacement for, the thin-sheet approach. Additionally, the single-camera thick-laser-sheet approach has also been shown to be a valuable tool for visualizing transitional flow structures.

Acknowledgments

We wish to acknowledge the contribution to this project from the NASA Langley Research Center 31-Inch Mach 10 Air Tunnel technicians and engineers, including Kevin Hollingsworth, Paul Tucker, Tony Robbins, Henry Fitzgerald and Johnny Ellis. This work was supported by the NASA Fundamental Aeronautics Hypersonics Program as well as NASA's Constellation Orion CEV Aeroscience Program (CAP). Thanks also to Rich Schwartz and Andrew McCrea from ATK Space Division, Hampton Virginia, Christopher Ivey, from Johns Hopkins University, and Danny Barrows, from the NASA Langley Research Center for assisting with the computer visualizations of the data.

References

[1] S. A. Berry, R. J. Nowak, and T. J. Horvath, "Boundary Layer Control for Hypersonic Airbreathing Vehicles," AIAA Paper Number 2004-2246, 34th AIAA Fluid Dynamics Conference and Exhibit, June 28 – July 1, 2004, Portland, Oregon, 2004.

[2] S. A. Berry, T. J. Horvath, A. M. Cassady, B. S. Kirk, K.C. Wang, and A. J. Hyatt, "Boundary Layer Transition Results From STS-114," 9th AIAA/ASME Joint Thermophysics and Heat Transfer Conference, AIAA-2006-2922, June, 2006.

[3] G. Kychakoff, P. H. Paul, I. Van Cruyningen, and R. K. Hanson, "Movies and 3-D Images of Flowfields Using Planar Laser-Induced Fluorescence," App. Optics, Vol. 26, pp. 2498-2500, 1987.

[4] B. Yip, R. L. Schmitt, and M. B. Long, "Instantaneous three-dimensional concentration measurements in turbulent jets and flames," Opt. Lett. **13**, 96-99, 1988.

[5] B. J. Patrie, J. M. Seitzman, and R. K. Hanson, "Instantaneous Three-Dimensional Flow Visualization by Rapid Acquisition of Multiple Planar Flow Images," Opt. Eng., vol. 33, pp. 975-980, 1994.

[6] F. Ossler, S. Agrup and M. Alden "Three-dimensional flow visualization with picosecond Mie scattering and streak-camera detection" Applied Optics Vol. 34, No. 3 , pp. 537-540, 20 January 1995.

[7] J. E. Goldstein and A. J. Smits, "Flow Visualization of the Three-Dimensional, Time-Evolving Structure of a Turbulent Boundary Layer," Phys. Fluids, Vol. 6, pp. 577-587, 1994.

[8] T. C. Island, B. J. Patrie, M. G. Mungal, and R. K.. Hanson, "Instantaneous Three-Dimensional Flow Visualization of a Supersonic Mixing Layer," Exp. Fluids, Vol. 20, pp. 249-256, 1996.

[9] J. Hult, A. Omrane, J. Nygren, C. F. Kaminski, B. Axelsson, R. Collin, P.-E. Bengtsson, and M. Alden, "Quantitative Three-Dimensional Imaging of Soot Volume Fraction in Turbulent Non-Premixed Flames," Exp. Fluids, Vol. 33, pp. 265-69, 2002.

[10] B. S. Thurow, "Recent Progress Towards a High-Speed Three-Dimensional Flow Visualization Technique", 22nd International Congress on Instrumentation in Aerospace Simulation Facilities, Pacific Grove, CA, June 10 – 14th, 2007.

[11] E.D. Torniainen, A. Hinz, and F. C. Gouldin, "Tomographic Analysis of Unsteady Reacting Flows," AIAA Journal, vol. 36, p. 1270-1278, 1998.

[12] C. J. Elkins, M. Markl, N. Pelc, and J. K. Eaton, "4D Magnetic resonance velocimetry for mean velocity measurements in complex turbulent flows," Exp. Fluids, Vol. 34, pp. 494-503, 2003.

[13] R. Snyder and L. Hesselink "Measurement of mixing fluid flows with optical tomography" Optics Letters, Vol. 13, No. 2, 87-89, February, 1988.

[14] W. B. Ng, Y. Zhang "Stereoscopic imaging and reconstruction of the 3D geometry of flame surfaces," Experiments in Fluids, Springer Berlin / Heidelberg , Vol. 34, No. 4, pp. 484-493, April, 2003.

[15] W.B. Ng, K.J. Syed and Y. Zhang, "The study of flame dynamics and structures in an industrial-scale gas turbine combustor using digital data processing and computer vision techniques," Experimental Thermal and Fluid Science Volume 29, Issue 6, pp. 715-723, July, 2005.

[16] K. Y. Cheung and Y. Zhang "Stereo imaging and analysis of combustion process in a gas turbine combustor" Meas. Sci. Technol. V. 17, pp. 3221-3228, 2006.

[17] P.M. Danehy, A.P. Garcia, S. Borg, A.A. Dyakonov, S.A. Berry, J.A. Wilkes Inman, D.W. Alderfer, "Fluorescence visualization of hypersonic flow past triangular and rectangular boundary-layer trips", AIAA-2007-0536, 45th AIAA Aerospace Sciences Meeting, Reno Nevada, January 8-11, 2007.

[18] B. F. Bathel, P. M. Danehy, J. A. Inman, D. W. Alderfer, S. A. Berry, "PLIF Visualization of Active Control of Hypersonic Boundary Layers Using Blowing", Paper Number 2008-4266, 26th AIAA Aerodynamic Measurement Technology and Ground Testing Conference, Seattle, WA June 23-26, 2008.

[19] J. R. Micol "Langley Aerothermodynamic Facilities Complex: Enhancements and Testing Capabilities," AIAA Paper 98-0147, 36th AIAA Aerospace Sciences Meeting & Exhibit, January 12-15, Reno, NV, 1998.

[20] Hollis, B.R. "Real-gas flow properties for NASA Langley Research Center Aerothermodynamics Facilities Complex Wind Tunnels," NASA Contractor Report 4755, Sept. 1996.

[21] D.W. Alderfer, P.M. Danehy, J.A. Wilkes Inman, K.T. Berger, G.M. Buck, and R. J. Schwartz, "Fluorescence Visualization of Hypersonic Flow Over Rapid Prototype Wind-Tunnel Models" AIAA Paper 2007-1063, 45th AIAA Aerospace Sciences Meeting and Exhibit, Reno, Nevada, Jan. 8-11, 2007.

[22] J. A. Inman, P.M. Danehy, R.J. Nowak, D.W. Alderfer, "Fluorescence Imaging Study of Impinging Underexpanded Jets" AIAA-2008-619, 46th AIAA Aerospace Sciences Meeting and Exhibit, Reno, Nevada, Jan. 7-10, 2008.

[23] J. A. Wilkes, D. W. Alderfer, S. B. Jones, and P. M. Danehy, "Portable Fluorescence Imaging System for Hypersonic Flow Facilities," *JANNAF Interagency Propulsion Committee Meeting*, Colorado Springs, Colorado, December, 2003.

[24] R. J. Schwartz, "ViDI: Virtual Diagnostics Interface Volume 1-The Future of Wind Tunnel Testing" Contractor Report NASA/CR-2003-212667, December, 2003.

[25] Autodesk 3ds Max Product Information, Autodesk Inc., http://usa.autodesk.com/adsk/servlet/index?id=5659302&siteID=123112, viewed Jan 2, 2006.

[26] "Matlab Central, An open exchange for the MATLAB and Simulink user community", Mathworks Corporation, http://www.mathworks.com/matlabcentral/fileexchange/loadFile.do?objectId=4977&objectType=FILE, viewed June 15, 2008.

[27] J. A. Inman, P. M. Danehy, R. J. Nowak, D. Alderfer, "Identification of Instability Modes of Transition in Underexpanded Jets," Paper Number 2008-4389, 38th AIAA Fluid Dynamics Conference, Seattle, WA June 23-26, 2008.